Journal of Computational Science 24 (2018) 91–100

Contents lists available at ScienceDirect

Journal of Computational Science

journal homepage: www.elsevier.com/locate/jocs

Impact of patient-specific LVOT inflow profiles on aortic valve prosthesis and ascending aorta hemodynamics

Jan Bruening[d,*], Florian Hellmeier[d], Pavlo Yevtushenko[d], Marcus Kelm[a], Sarah Nordmeyer[a], Simon H. Sündermann[c], Titus Kuehne[a,b,d], Leonid Goubergrits[d]

[a] Department of Congenital Heart Disease and Paediatric Cardiology, Deutsches Herzzentrum Berlin, Augustenburger Platz 1, 13353 Berlin, Germany
[b] Department of Paediatric Cardiology, Charité – Universitätsmedizin Berlin, Augustenburger Platz 1, 13353 Berlin, Germany
[c] Department of Cardiothoracic and Vascular Surgery, Deutsches Herzzentrum Berlin, Augustenburger Platz 1, 13353 Berlin, Germany
[d] Institute for Computational and Imaging Science in Cardiovascular Medicine, Charité – Universitätsmedizin Berlin, Augustenburger Platz 1, 13353 Berlin, Germany

ARTICLE INFO

Article history:
Received 29 December 2016
Received in revised form
13 September 2017
Accepted 7 November 2017
Available online 8 November 2017

Keywords:
Virtual treatment planning
Patient-specific haemodynamics
Image-based computational fluid dynamics
Aortic haemodynamics
Cardiovascular modelling
Heart valve prosthesis

ABSTRACT

Patient-specific models become increasingly important in cardiovascular research as they allow prediction of surgical procedures. While the left ventricular outflow profile is an essential boundary condition, it remains unknown before treatment takes place. To overcome this problem, hemodynamics after virtual valve replacement were calculated based on different inlet profiles at the left ventricular outflow tract: a generic plug profile and a profile derived from 4D-flow-MRI. Spatially averaged parameters within the aorta were not significantly altered using either profile. A generic profile might be sufficient for the prediction of hemodynamics, circumventing the problem of predicting change in patient-specific boundary conditions.

© 2017 Elsevier B.V. All rights reserved.

1. Introduction

The assessment of hemodynamics using continuously developing computational fluid dynamics (CFD) is playing an increasing role in the understanding of cardiovascular processes and diseases [36]. The possibility of spatially and temporally well resolved analysis of hemodynamics without any need for invasiveness is one of the reasons that CFD provides ideal assistance in cardiovascular research. Furthermore, patient-specific planning of different treatment modalities might be feasible in clinics within the near future. Thus, different treatment strategies for a specific patient and disease might be investigated and tested in-silico before the actual treatment procedure.

A requirement for using CFD in patient-specific analysis or treatment planning is that the reconstruction of the cardiovascular system's anatomy is feasible with imaging techniques such as magnetic resonance imaging (MRI) and x-ray computed tomography (CT). However, specification of patient-specific inlet boundary conditions is often difficult due to lack of information about hemodynamics within the patient. Therefore, generalized boundary conditions, such as parabolic or constant inlet velocity (plug) profiles and literature-based flow rates, were commonly used in the past [15,25].

Due to an increased availability of modern imaging techniques in a clinical workflow, as for example four-dimensional velocity encoded MRI (4D-VEC-MRI), acquisition of patient-specific flow conditions and velocity profiles became possible [1,11,30]. Recent studies suggest that incorporation of patient-specific velocity profiles as inflow boundary condition improves accuracy of CFD-based analysis of cardiovascular hemodynamics [6,17,28]. For example, usage of patient-specific inflow profiles resulted in an overall more helical flow, increased wall shear stress and a significant reduction of predicted pressure losses in simulations of aortic coarctations, compared to simulations using generic inflow profiles [17]. Consequently, more recent studies incorporate patient-specific inlet boundary conditions into image-based CFD-workflows [38].

Thus, usage of patient-specific inflow profiles should be favoured for numerical investigation of cardiovascular dis-

* Corresponding author at: Biofluid Mechanics Laboratory, Institute for Computational and Imaging Science in Cardiovascular Medicine, Charité – Universitätsmedizin Berlin, Augustenburger Platz 1, 13354 Berlin, Germany.
E-mail address: jan.bruening@charite.de (J. Bruening).

https://doi.org/10.1016/j.jocs.2017.11.005
1877-7503/© 2017 Elsevier B.V. All rights reserved.

eases. However, when performing predictive treatment planning, patient-specific inflow profiles might not always be available. In general, use of clinically acquired flow data is challenging due to a lower resolution of 4D-flow-MRI data compared to anatomical MRI or CT data [17]. Since data of different MRI sequences for flow and anatomy have to be used, additional steps for data registration are required. These steps might be a source of additional errors. Misalignment between the MRI data sets for anatomy and flow might result in misaligned inflow profiles. Due to the measured noise within the 4D-flow-MRI sequence, velocities outside of the vessel lumen might be incorporated into the inlet velocity profile and thus result in additional errors during the simulation.

Recent studies indicate that flow patterns and parameters describing orientation and position, of the main flow within the ascending aorta correlate with diseases and remodelling of the aorta such as aneurysm growth and atherosclerosis [8,16,27]. Usually those patterns are divided into main and secondary flow patterns. While the main flow patterns characterize (through-plane) flow parallel to the vessel orientation, as for example the jet eccentricity, secondary flow patterns, as for example swirl, recirculation and helicity characterize flow perpendicular to the vessel orientation (in-plane). However, no clinically relevant thresholds of these parameters were defined as of yet. Nonetheless, it might be beneficial to consider these parameters upon judging the success of a specific treatment in the future. While those parameters can be measured in-vivo using 4D-flow-MRI, predicting their change after treatment is not yet possible.

A general aim is the development a methodology for virtual aortic valve treatment, which allows prediction of hemodynamic changes due to treatment of diseased aortic valves. This methodology requires modelling of the left ventricular outflow tract (LVOT), the aortic valve prosthesis and the aorta. As mentioned before, patient-specific velocity inlet profiles within the LVOT could affect accuracy and outcome of predicted post-treatment hemodynamics. However, an aortic valve replacement procedure might alter the ventricular function as well as the LVOT's geometry and thus the hemodynamics within the LVOT severely. These changes, and therefore patient-specific boundary conditions as well, are not known a priori and there is no way to predict them as of yet.

The presented study focusses on the impact of chosen velocity inflow profiles at the LVOT on estimated hemodynamics after a patient-specific aortic valve replacement procedure. Desirably, the choice of velocity inflow profiles has no or only minor impact on these predicted hemodynamics. This study's hypothesis is that position, size and type of the aortic valve are the main contributors in defining aortic hemodynamics. It is hypothesized that the impact of the chosen velocity inlet profile on these hemodynamics is only of minor importance, since the valve prosthesis itself strongly affects and sculpts the hemodynamics. The transition from the vascular tissue toward the artificial valve prosthesis is usually not smooth. Disturbances caused at the junctions between tissue and prosthesis as well as the non-physiologic shape of the prostheses might have a higher impact on the aortic flow than the variability of flow profiles within the LVOT, upstream of the prosthesis. If this assumption is valid, usage of generic non-patient-specific velocity inlet profiles might be used for prediction of hemodynamic outcome after replacement of a diseased aortic valve.

In order to understand the impact of LVOT inflow conditions on the aortic valve and the ascending aorta hemodynamics, an MRI-based CFD study of an aortic valve replacement procedure with mechanical or biological valve prostheses in ten patients was performed. A generic plug inlet velocity profile was compared against patient-specific LVOT velocity inlet profiles. Hemodynamic parameters characterizing valve prosthesis function and aortic flow were compared.

2. Materials and methods

2.1. Study population

Ten patients, who underwent aortic valve replacement, were included within this retrospective study. Treatment of these patients was performed at the Department of Congenital Heart Disease and Pediatric Cardiology of the German Heart Institute Berlin. All but one patient were male and the mean age of this sample was 41 years. Six patients received a mechanical and three patients a biological valve prosthesis. In the remaining patient, the diseased aortic valve was replaced using his autologous pulmonary valve (Ross procedure). Detailed information is provided in Table 1. Informed consent was signed by all patients and usage of retrospective imaging data was approved by the responsible institutional review board.

2.2. Imaging data

Conventional as well as velocity encoded (4D-flow) MRI images were acquired within one scanning session using a 1.5 Tesla Achieva MRI scanner (Philips Medical Systems, Best, The Netherlands). Reconstructed voxel sizes were equal to or below $1.8 \times 1.8 \times 2.0$ mm^3 for conventional MRI images (see Table 1 for exact values), while the spatial resolution of 4D-flow-MRI images was $2.3 \times 2.3 \times 2.8$ mm^3. Conventional MRI sequences for reconstruction of the anatomy were only acquired for the end-diastolic state, while the 4D-flow-MRI sequence for measuring the patient-specific hemodynamics had a temporal resolution of 1/25th of the cardiac cycle.

Table 1
Overview of patients included within this study. The patients' age and sex are specified as well as the type of vascular and valve prosthesis used during surgical valve replacement. The diameter specified equals the nominal size of the valve prosthesis according to the manufacturer's information. In case of patient 02 the diameter equals the inner diameter of the valve prosthesis. If a vascular graft was used to replace the ascending aorta, the graft type and diameter used are specified. Since spatial resolutions for conventional MRI data varied between patients, the resolution is specified as well.

Patient			Aortic Valve Prosthesis				Vasclular Graft	MRI information
ID	Sex	Age	Type	Manufacturer	Model	Diameter	Type, Diameter	Voxel resolution
01	M	18	mech.	St. Jude Medical	Regent	25 mm	none	$1.42 \times 1.42 \times 2\ mm^3$
02	M	15	biol.	autologous pulmonary valve	–	25 mm	none	$1.42 \times 1.42 \times 2\ mm^3$
03	M	32	mech.	St. Jude Medical	Regent	25 mm	Hemashield, 32 mm	$1.42 \times 1.42 \times 2\ mm^3$
04	M	67	biol.	Carpentier Edwards	Magna Ease	21 mm	none	$1.83 \times 1.83 \times 2\ mm^3$
05	M	20	mech.	St. Jude Medical	Regent	25 mm	Hemashield, 30 mm	$1.42 \times 1.42 \times 2\ mm^3$
06	M	50	biol.	Carpentier Edwards	Magna Ease	25 mm	none	$1.42 \times 1.42 \times 2\ mm^3$
07	F	61	biol.	Medtronic	Hancock II	21 mm	none	$1.42 \times 1.42 \times 2\ mm^3$
08	M	13	mech.	Medtronic	Open Pivot	21 mm	Hemashield, 24 mm	$1.39 \times 1.39 \times 2\ mm^3$
09	M	71	mech.	St. Jude Medical	Regent	23 mm	none	$0.91 \times 0.91 \times 2\ mm^3$
10	M	60	mech.	Medtronic	Open Pivot	25 mm	none	$0.61 \times 0.61 \times 2\ mm^3$

2.3. Segmentation

Pre-interventional, patient-specific geometries of the left ventricular outflow tract, as well as the aorta, including the ascending aorta, the aortic arch and the descending aorta, were segmented from conventional MRI images. Due to the resolution of the conventional MRI images, the thin leaflets of the aortic valve could not be segmented. Therefore, the pre-interventional state of the aortic valve could not be reconstructed. The segmentation was performed mostly manually using ZIBAmira (v. 2015.28, Zuse Institute Berlin, Germany). Rough surface geometries were then created from segmentations and subsequently smoothed using ReMESH (v. 2.0, IMATI, Genoa, Italy). This segmentation process has been described in detail earlier [17].

2.4. Virtual intervention

Virtual interventions were performed by altering pre-interventional patient-specific geometries obtained after segmentation and subsequent smoothing. Those geometries were altered according to surgery reports of real interventions performed on patients. In all ten cases a geometry of the aortic valve prosthesis used during surgery was virtually implanted within the aortic geometry. To facilitate this, the region surrounding the original aortic valve annulus was removed from the vessel geometry by cuts perpendicular to the vessel orientation and the corresponding valve prosthesis geometry was then inserted and aligned within this cut off region using ZIBAmira. The size of the removed region was chosen in respect to the chosen prosthesis type to ensure, that the gap created was big enough for the artificial valve. Afterwards, the valve prosthesis geometries were stitched to the aortic bulbus as well as the left ventricular outflow tract (LVOT) using GAMBIT (v. 2.4.6, ANSYS, Inc., Canonsburg, USA).

Both mechanical valve prosthesis models used within this study were reverse-engineered using SolidWorks (v. 2011, Dassault Systèmes, Vélizy-Villacoublay, France). The prostheses' geometries were reconstructed from the advertising brochures and manuals both manufacturers provide on their respective websites. Measures, such as the inner and outer diameters of the prostheses, were derived from these sources as well. The opening angles of both prostheses were not specified by the manufacturer. Therefore, measurements by Dumont et al. were used to correctly model the opening angles of both bi-leaflet prostheses [9]. All valves were modelled in a fully opened position and details of the leaflets' hinges were not considered. Mechanical valves were rotated within the valve region, so that leaflets were parallel to the cardiac septum. This is the usual orientation of mechanical aortic valve prostheses during surgery [31].

Biological valve prostheses used for treatment of three patients were modelled using an optically scanned Fisics-Incor valve (INCOR, Hospital das Clínicas, University of São Paulo, São Paulo, Brazil) [35]. This valve was scanned in a completely opened position as well. Biological valve prostheses were rotated to align the valve leaflets with the three aortic sinuses. This procedure is exemplarily shown in Fig. 1A for a biological valve prosthesis.

For one patient, no artificial valve prosthesis, but the autologous pulmonary valve of that patient was used to replace the aortic valve. This valve was modelled in SolidWorks using a geometric definition of tri-leaflet aortic valves proposed by [24].

If a vascular graft was implanted during surgery, a bent tube with matching constant diameter and position was created using ZIBAmira. The aortic section replaced during surgery was cut off the virtual aortic geometry as well. The artificial tube was then stitched to remaining parts of the vessel using GAMBIT (v. 2.4.6, ANSYS, Inc., Canonsburg, USA). This procedure was performed for the patients 03, 05 and 08.

2.5. Mesh generation

Generation of computational meshes was performed using GAMBIT. A node distance of approximately 0.6 mm was specified for the complete volume downstream of the aortic valve. Here, a boundary layer consisting of three prism cell layers was specified. The first layer's height was set to 20 percent of the node distance,

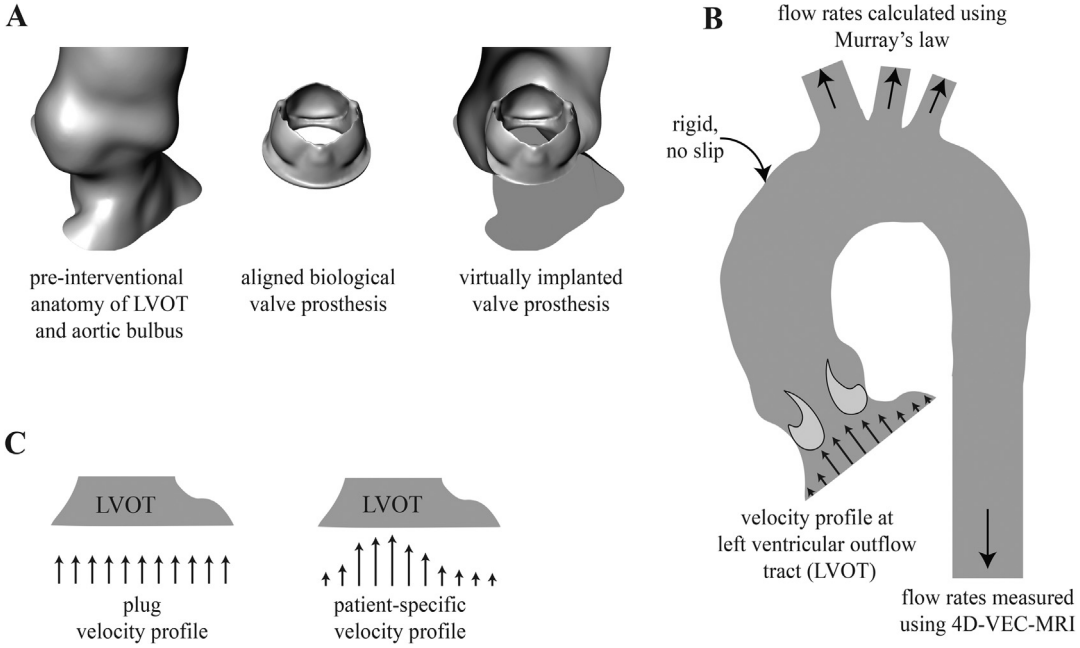

Fig. 1. Visualization of the geometry of a virtual valve prosthesis equal to the model used within the real surgical intervention aligned and stitched to the aortic root (A). The numerical domain is shown together with chosen boundary conditions (B). At the left ventricular outflow tract (LVOT) either an idealized plug velocity profile with a constant velocity or a patient-specific velocity profiles extracted from 4D-flow-MRI was specified (C).

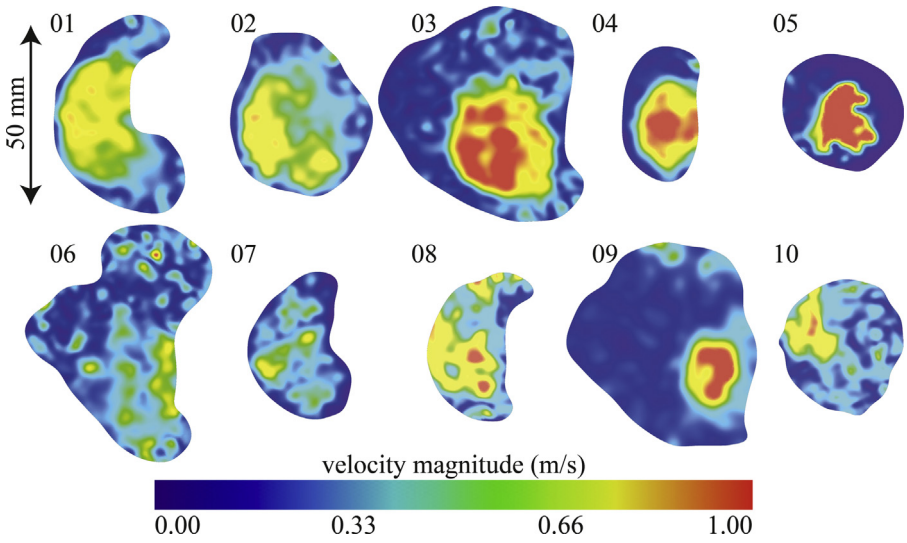

Fig. 2. Visualization of inlet boundary shapes and velocity magnitudes of patient-specific inlet profiles derived from 4D-flow-MRI. The scale for all ten geometries is identical. All geometries were rotated in a way that the observer looks from the ventricle into the aorta. The mitral valve would be positioned right of the profiles.

while the subsequent layer's height increased by a factor of 1.2. A node distance of approximately 0.2 mm was specified within the aortic root to compensate for the lack of a boundary layer, which could not be applied due to the complex geometries of the aortic valve prostheses used. The resolution used was shown to be sufficient for mesh independent results within the ascending aorta [17]. A mesh independency study for the presented numerical setup indicated, that the resolution was sufficient for mesh independent results of the transvalvular pressure drop, which varied less than one percent using higher resolutions, as well as derivatives of the flow field as for example the wall shear stresses. Details on the meshes were depicted in earlier work [20].

2.6. Assessment of patient-specific velocity inlet profiles

Using GTFlow (gyroTools LLC, Zurich, Switzerland), peak flow rates at the ascending and descending aorta were acquired from 4D-flow-MRI images. Extraction of patient-specific velocity inlet profiles at the LVOT was performed using MEVISFlow (v. 9.0, Fraunhofer MEVIS, Bremen, Germany). Segmentation of the aorta using 4D-flow-MRI data is difficult. However, a segmented geometry is necessary to correctly define the position of the LVOT plane. Therefore, a binary DICOM image stack was created using the virtually treated geometry. These images were loaded into MEVISFlow together with the 4D-flow-MRI images. Firstly, the alignment of 4D-flow and conventional MRI images was checked and an interactive registration was performed if necessary. Thus, the correct position of the plane for extraction of the velocity inlet profiles could easily be determined. After this registration step, the velocity inlet profile was exported as a set of 3D velocity vectors within the plane chosen in MEVISflow. Those velocity vector components were then interpolated onto the vertices of the LVOT inlet boundary using ZIBAmira. The shape of the LVOT inlet boundary as well as the velocity inlet profile for each patient are shown in Fig. 2.

2.7. Computational fluid dynamics

Steady-state simulations of the peak-systolic aortic flow were performed using ANSYS Fluent (v. 16.1, ANSYS, Inc., Canonsburg, USA). Vessel walls as well as the valve prosthesis were assumed to be rigid, and a no-slip boundary condition was applied at all walls. An outflow boundary condition was specified for each truncating branching vessel of the aortic arch, as well as the descending aorta. While the flow rates within the ascending and descend-

Table 2
Overview of parameters calculated for each patient. Reynold's numbers were calculated using the average flow velocity, kinematic viscosity of $3.33 \cdot 10^{-6}$ m^2/s and the nominal prosthesis diameter (see Table 1). Coefficients of determination were calculated for WSS as well as velocity magnitudes. Pressure drops across the aortic valve (Δp), the normalized flow displacement (NFD) as well as the secondary flow degree (SFD) within the ascending and descending aorta were calculated. Surface-averaged WSS within the ascending aorta and averaged turbulent kinetic energy (TKE) were evaluated for both conditions.

ID	Re	R^2 [1]		Δp [mmHg]		NFD [1]		SFD_{AoAsc} [1]		SFD_{AoDecs} [1]		$WSS_{Avg,Asc}$ [Pa]		TKE [cm^2/s^2]	
		vel.	WSS	MRI	plug	MRI	plug	MRI	plug	MRI	plug	MRI	plug	MRI	plug
01	11,800	0.776	0.819	6.3	7.8	0.095	0.091	0.70	0.74	0.11	0.17	20.7	19.3	250	210
02	6300	0.779	0.835	3.1	3.2	0.112	0.105	0.37	0.37	0.33	0.28	13.9	13.2	148	79
03	3850	0.675	0.627	8.6	12.1	0.029	0.025	0.85	0.89	0.16	0.15	15.5	18.4	350	20
04	4800	0.572	0.694	0.9	2.8	0.016	0.030	0.33	0.33	0.18	0.15	5.9	6.6	53	60
05	4250	0.339	0.458	1.4	3.9	0.092	0.048	0.57	0.59	0.15	0.29	5.6	4.3	350	20
06	3200	0.385	0.486	5.0	8.4	0.016	0.070	1.21	1.06	0.26	0.32	6.2	8.5	115	84
07	5400	0.723	0.658	6.2	7.8	0.021	0.030	1.54	1.53	0.53	0.54	4.5	4.9	117	146
08	3300	0.729	0.759	34.6	40.5	0.098	0.126	0.96	0.98	0.12	0.29	50.2	47.6	712	653
09	4650	0.388	0.535	4.5	13.7	0.066	0.137	0.81	1.00	0.62	0.64	15.1	12.0	245	112
10	2300	0.494	0.503	9.9	12.5	0.074	0.099	1.12	1.12	0.10	0.10	5.6	8.6	185	185
mean	5000	0.586	0.637	8.0	11.3	0.062	0.0760	0.84	0.86	0.26	0.29	14.3	14.3	232	167
SD	2650	0.173	0.139	9.7	11.0	0.038	0.0416	0.38	0.36	0.16	0.17	13.8	12.8	189	180
p-value			**0.002 (STT)**		.203 (STT)		.235 (WSR)		.577 (STT)		0.978 (WSR)		**0.021 (WSR)**		

For all parameters featuring significant differences, p-values were highlighted using bold text.

ing aorta was measured using 4D-flow-MRI, flow rates flowing off through the branching vessels of the aortic arch were modelled using Murray's Law [29]. This setup is visualized in Fig. 1B. To model turbulence observed within systolic aortic hemodynamics [21], a standard k-omega SST turbulence model with a turbulence intensity of 5 percent at the velocity inlet was applied. The use of a turbulence model is indicated, since mean Reynolds numbers for the 10 cases simulated was 5000 (see Table 2). While the turbulence model used is not ideally suited for calculation of turbulence parameters, it is sufficient for calculation of hemodynamic parameters investigated in this study, as for example the pressure drop [22] and the wall shear stresses [34]. Blood was modelled as a non-Newtonian fluid with a constant density of 1050 kg/m^3 and a shear rate dependent viscosity [37]. For high shear rates above 1000 s^{-1}, the dynamic viscosity was 3.5 mPa s. Even though the rheology model used has only a minor impact on flow simulations during peak systole [23], modelling the non-Newtonian behaviour of blood reproduces in-vivo conditions, reducing additional uncertainty in the results [26].

At the LVOT, a velocity inlet boundary condition was applied using either a plug velocity profile or the patient-specific velocity profile extracted from 4D-flow-MRI using MEVISFlow (see Fig. 1C).

2.8. Qualitative and quantitative analysis of hemodynamics

The flow within the valve prostheses and aorta was visualized using ZIBAmira. Streamlines seeded from the LVOT were used as well as velocity magnitude profiles immediately downstream the aortic valve prosthesis. Besides this qualitative comparison of hemodynamics calculated using both velocity inlet profiles, quantitative comparison of relevant flow parameters was performed as well. The pressure drop across the valve prosthesis was calculated using ZIBAmira. A centerline with evenly distributed nodes of 0.1 mm distance was generated. The static pressure field calculated using CFD was averaged, so that each node of the centerline represented the respective average cross-section pressure within the aorta. The surface averaged wall shear stress within the ascending aorta was calculated for all cases as well as the secondary flow degree within one cross section of the ascending and descending aorta. The secondary flow degree is an index describing the "straightness" of tubular flow and is defined as the ratio of the average in plane velocity and the average through plane velocity in one chosen plane. Furthermore, the normalized flow displacement (NFD) was evaluated. This parameter, which is defined as the difference between the center of the vessel and the center of the flow, normalized by the vessel diameter [32], was evaluated in an aortic cross section, which was oriented at the cranial border of the right pulmonary artery.

Since numerical meshes used for simulations with plug and patient-specific velocity inlet profiles were identical, cell-wise comparison of flow parameters between both velocity inlet profile conditions was feasible. Correlation coefficients between velocity, magnitudes as well as the wall shear stresses calculated using both inlet profiles, were evaluated as means to describe spatially resolved similarity within the flow fields.

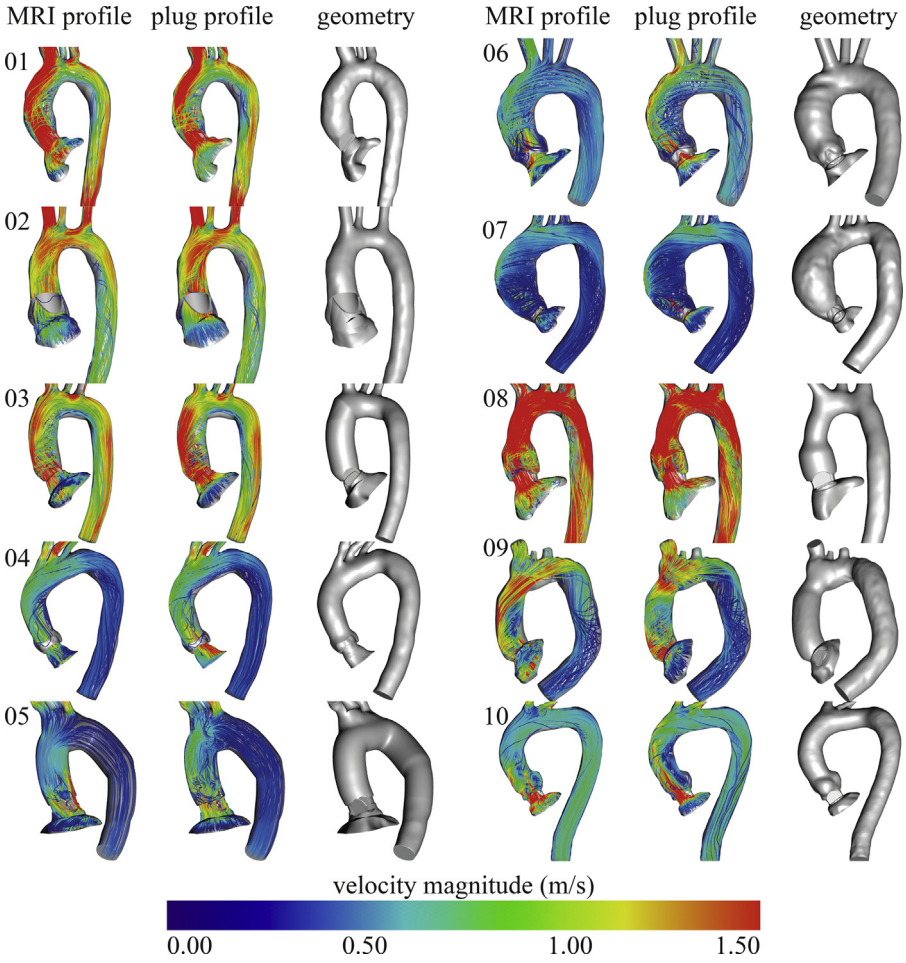

Fig. 3. Visualization of hemodynamics calculated using either the patient-specific (left) or the plug (middle) velocity inlet profile using streamlines which are colored according to the velocity magnitudes. Additionally, the virtually treated geometry is shown for each patient (right).

2.9. Statistical analysis

Statistical analysis was performed using SPSS version 23 (IBM, Armonk, USA). Differences in all parameters calculated using both inlet profiles were tested for normal distribution using the Shapiro-Wilk test. Student's *t*-test (STT) was then used to test for significant differences within normally distributed parameter differences, while the Wilcoxon signed rank test (WSR) was used for testing non-normally distributed parameter differences. All tests used a standard significance level of 0.05 and were performed two-sided.

3. Results

3.1. Qualitative comparison of hemodynamics

Hemodynamic outcomes calculated using either the constant plug or the patient-specific velocity inlet profile are shown in Fig. 3 visualized by using streamlines, which are colour coded using the velocity magnitude. The virtually treated aortic geometry is shown as well to indicate orientation and rotation of the valve prostheses used in relation to the vessel geometry. Even though this is only a qualitative comparison, notable differences between hemodynamics calculated using both conditions could be found in some patients, while there were hardly any differences in other patients.

In patient 04, differences in flow patterns and velocity magnitudes could be observed within the LVOT as well as the vicinity of the valve prosthesis. The plug inlet condition resulted in higher velocities near the wall of the LVOT. However, no distinct hemodynamic differences within the ascending aorta or the aortic arch were observed between both conditions. An overall more equally distributed blood flow across the valve prosthesis of patient 05 could be observed using the plug inlet condition. Using the MRI inlet condition, a jet was passing between one leaflet of the mechanical prosthesis and the aortic wall, resulting in the flow being attached to opposite sites in both conditions. Blood flow in the ascending aorta of the plug inlet condition featured more swirls and was overall less straight. In patient 06 a distinct jet could be seen in the MRI inlet condition. This jet, which is formed by the biological valve prosthesis, was oriented along the center of the ascending aorta. Even though, using a plug inlet profile resulted in a jet as well, that jet was oriented directly at the aortic wall, resulting in high velocity magnitudes near the wall as well as a recirculation featuring velocity magnitudes near zero. Although orientation of streamlines near the wall was the same for both conditions in patient 09, the ascending aorta hemodynamics featured distinctive differences. Using a plug inlet profile resulted in a bigger recirculation zone. In patient 10 a jet was predicted using a plug inlet profile. While a jet could also be observed using the patient-specific profile, this jet was shorter and fanned out quickly. Therefore, the large recirculation region in the ascending aorta, observed using the plug inlet condition, was not present using the patient-specific velocity inlet. Qualitative comparison of flow fields in the descending aorta revealed no clear differences in any patient.

3.2. Quantitative comparison of hemodynamics

These findings agreed with quantitative comparison of flow field. Cell-wise correlations and corresponding coefficients of determination (R^2) were calculated for WSS as well as velocity magnitudes (see Table 2). The average coefficient of determination for WSS calculated using both methods was $R^2_{WSS} = 0.59$, while the average coefficient for velocity magnitudes was $R^2_{velocity} = 0.64$. However, coefficients calculated for individual patients varied individually and ranged from $0.34 < R^2_{WSS} < 0.78$ and $0.46 < R^2_{velocity} < 0.84$ respectively. Therefore, differences between hemodynamics calculated using both inlet conditions were bigger in some patients than in others. In patients were a qualitative comparison already revealed hemodynamic differences, relatively low coefficients of determination were observed: patients 04, 05, 09 and 10. However, coefficients of determination calculated for patient 06 were below 0.5 as well, indicating low agreement between hemodynamics calculated using both inlet profiles.

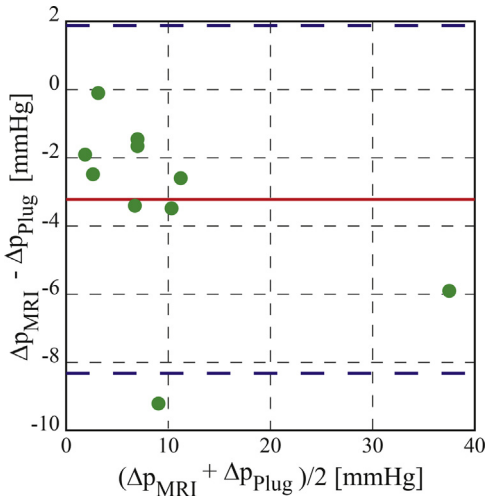

Fig. 4. Bland-Altman-diagram for visualization of the differences in the pressure drop calculated both inlet profiles.

According to the Shapiro-Wilk test, the following parameter differences between both conditions were not normally distributed ($p < 0.05$): secondary flow degree within the ascending aorta (SFD_{AoAsc}), averaged turbulent kinetic energy (*TKE*). Consequently, differences in the pressure drop across the valve prosthesis (Δp), the surface-averaged wall shear stress ($WSS_{Avg,Asc}$), the normalized flow displacement (NFD), as well as the secondary flow degree in the descending aorta (SFD_{AoDesc}) and the normalized flow displacement were normally distributed.

Using a plug velocity inlet profile resulted in a significant increase in the pressure drop across the valve of 3.3 mmHg, compared to the MRI inlet profile condition (STT, $p = 0.002$). Furthermore, pressure drops calculated using both methods correlated significantly ($R^2 = 0.96$, $p < 0.001$) (Fig. 4).

Volume-averaged TKE was significantly increased in simulations using a MRI inlet profile compared to the plug inlet profile condition (WSR, $p = 0.021$). In all other parameters, no significant difference between both conditions was observed.

3.3. Change in hemodynamics distally to the valve prostheses

To allow comparison of blood flow in the immediate vicinity of the valve, velocity magnitude profiles immediately downstream of the aortic valve prostheses were extracted and visualized (see Fig. 5). While qualitative comparison of hemodynamics within the whole aortic domain revealed good agreements in at least six out of ten patients, good agreements in velocity magnitude profiles downstream of the aortic valve prosthesis were only observed in patient 01, 03 and 07. In all other patients, notable differences between profiles calculated with either inlet profile was observed. These differences comprised shift of the velocity maximum, differences in velocity magnitudes and the shape of high velocity flow patterns. No relationship between the agreement of flow profiles downstream of the valve prosthesis and of the inlet profile (see Fig. 1) could be identified. While the inlet profile of patient 07 featured no clear center, profiles of patients 01 and 03 featured a distinct centered maximum. In all other cases, where the flow pro-

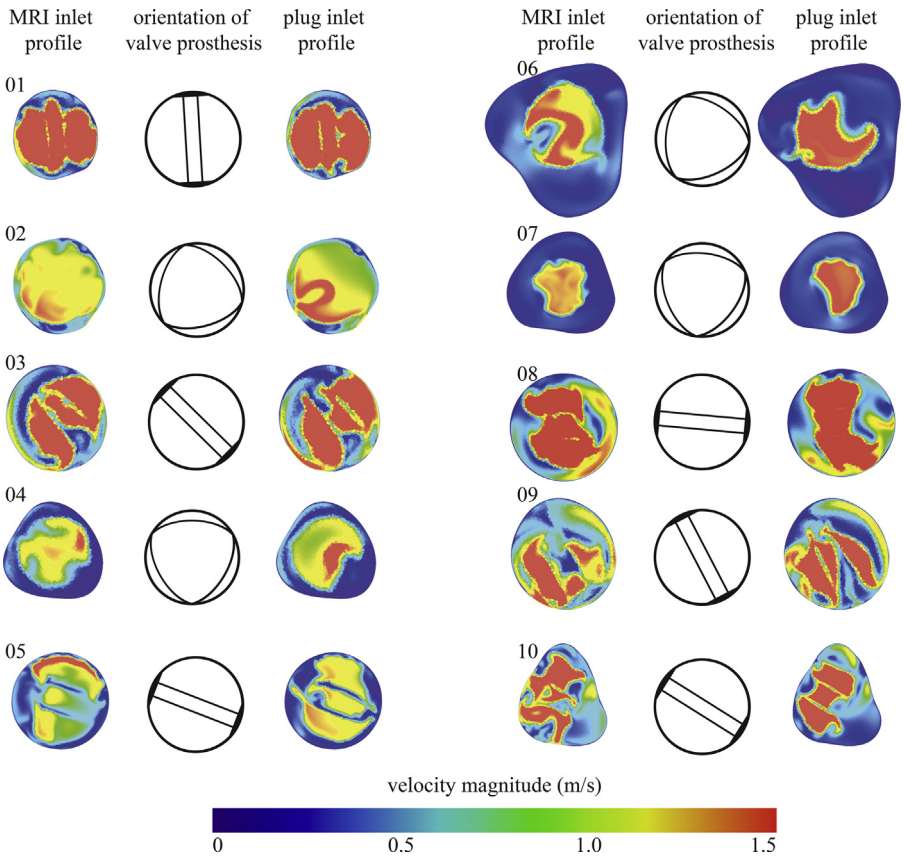

Fig. 5. Comparison of velocity magnitude profiles calculated using both velocity profile conditions. The profiles were evaluated at a cross section immediately after the valve. The distance between the leaflets' tips and the displayed cross section was approximately 5 mm. The orientation and type of the valve prosthesis used in each patient is indicated using a generic stencil.

files downstream of the prostheses calculated using both methods differed, no common feature of the inlet profiles could be identified either.

4. Discussion

While in some patients strong qualitative as well as quantitative similarity of hemodynamics calculated using both velocity inlet profiles was observed, these hemodynamics differed clearly in other patients. In four patients, correlation coefficients of wall shear stresses or velocity magnitudes below 0.5 were observed, revealing gross differences in calculated flow fields and thus indicating a non-neglectable effect of the velocity inlet profile choice towards spatially resolved numerical results.

Even though there was no ideal agreement in spatially resolved values in any patient, several spatially averaged parameters featured no significant difference between both velocity inlet conditions. This includes the SFD_{AoAsc} and SFD_{AoDesc}, as well as the NFD, which are averaged measures of orientation and position of the main flow. This indicates, that these features are mainly affected by the geometry of the aortic valve prostheses as well as the geometry of the aorta itself. Assessment of those parameters seems robust against changes in the velocity inlet profile used. However, whether the orientation and displacement of the flow is mainly defined by the aortic valve prosthesis or the aortic geometry cannot be determined using this approach.

While the interaction between hemodynamics and vascular remodelling is not fully understood as of yet, correlations between abnormal hemodynamics and aortic aneurysms, dilation and atherosclerosis were suggested [7,8,16,27]. Therefore, not only immediate measures as the transvalvular pressure drop should be taken into account when determining the success of an aortic valve replacement procedure. However, assessment of parameters describing the orientation and displacement of aortic blood flow became possible only recently. Clinically relevant thresholds and margins must yet be determined. Especially because secondary flow patterns were observed in healthy subjects as well [14,30]. First results suggest, for example, that the NFD correlates with future ascending aortic growth in patients suffering from bicuspid valve disease [5]. While assessment of these parameters is possible before and after the intervention using Echocardiography and 4D-flow-MRI, their prediction can only be facilitated using numerical methods. As this study suggests, using a generic plug inlet profile has no major impact on these parameters.

No significant differences within the surface-averaged WSS were found either. WSS are a measure for the interaction between blood and the vessel wall and correlate with exchange processes as well as the overall load acting on the endothelial cells. This finding, however, was to be expected, because volume flow rates in both velocity inlet profile conditions were identic and no significant differences in SFD were found. Nonetheless, low coefficients of determination for cell-wise comparison of WSS indicates, that there are large differences in spatially resolved WSS, even though the surface-averaged WSS are similar in both groups. WSS are associated with vascular diseases as well as remodelling [7,27]. A spatially resolved evaluation is not feasible using the method proposed in this study, since the choice of the velocity inlet profile has

a non-negligible impact on spatially resolved parameters such as the WSS.

There are two exemptions from the observation that spatially-averaged parameters calculated using either inlet profile condition agreed well: the transvalvular pressure drop and the averaged turbulent kinetic energy.

Using patient-specific velocity inlet profiles as boundary conditions resulted in significantly lower pressure drops across the aortic valve compared to those calculated using a plug profile. This peak systolic pressure drop is one essential parameter in evaluation of treatment success. Commonly, pressure drops equal or lower than 20 mmHg are considered normal. Higher pressure drops might indicate a possible stenosis of the prosthesis [39]. Thus, the observed average difference in pressure drop of 3.3 mmHg accounts for 16.5 percent of this clinical threshold. However, the transvalvular pressure drop is commonly estimated by measuring the velocity maximum downstream the valve using echocardiography. From these velocity measurements, a pressure drop is then calculated from the velocity magnitude distal to the prosthesis using a simplified Bernoulli equation: $\Delta p = v^2_{proximal} \cdot \frac{\mathrm{mmHg\,s^2}}{\mathrm{m^2}}$, or more accurately using the proximal velocity as well $\Delta p = \left(v^2_{distal} - v^2_{proximal}\right) \cdot \frac{\mathrm{mmHg\,s^2}}{\mathrm{m^2}}$ [2,39].

Thus, the pressure drop is only measured indirectly within clinical routine and is usually overpredicting the real pressure drop, because the pressure gain due to deceleration of the flow downstream the valve is not taken into account [3,39]. It is therefore necessary to validate transvalvular pressure drops calculated in-silico against those measured in-vivo. Since there was a nearly perfect correlation between pressure drops calculated using either inlet profile condition, using a plug inlet profile might be sufficient for prediction of unphysiologically high pressure drops. However, an adjustment of the clinical threshold might be necessary to take the overpredicting bias into account.

The average turbulent kinetic energy was significantly increased using the patient-specific velocity inlet profile compared to the plug profile. This finding was to be expected, since the patient-specific profiles usually feature a distinct velocity maximum and thus bigger velocity gradients, while there is no velocity gradient in the plug velocity profile at all. Recent studies found lower turbulence within physiologic hemodynamics compared to pathologic ones [10]. While prediction of turbulence after treatment might be desirable, no clinical thresholds and definitions of pathological degrees of turbulence are established as of yet. Furthermore, it is difficult to obtain reliable in-vivo data of turbulence because of limited access and measurement techniques. Howsoever, this study suggests that the velocity inlet profile has an impact on prediction of turbulence, which might not be negligible.

An important finding was that velocity magnitude profiles extracted immediately downstream of the aortic valve prostheses revealed distinct differences in all but three patients. While general flow orientation and displacement was not significantly different using either velocity inlet condition, hemodynamics in the immediate vicinity of the aortic valve prostheses were substantially different. Here, a limitation of the method used becomes clear. Valve prostheses were assumed to be ideally opened, regardless of pressure and flow patterns before the valve or the pressure distribution within the valve. Even though valve prostheses are designed to fully open during peak systole, it is possible that the clear differences of the blood flow within the immediate vicinity of the prostheses might lead to alterations in opening angles of leaflets of mechanical prostheses or leaflet geometries of biological prostheses. The method used within this study is not able to incorporate these influences of hemodynamics on the prosthesis geometry. It may be possible that leaflet angles and therefore the effective orifice area of valve prostheses might be altered by the chosen velocity inlet profile. However, according the ISO 5840, these prostheses are tested in-vitro within a straight tube. Even though a non-patient-specific flow or an anatomic geometry is used for these test, the prostheses' leaflets do open fully under these conditions. Nonetheless, additional research on the impact of different velocity inlet profiles on function on prostheses seems warranted. Here, fluid-structure-interaction models or immersed boundary approaches might be suited.

Ideally, results observed using this method should be validated against real clinical measures obtained after aortic valve replacement. However, validation of similarly simplified patient-specific simulations of aortic hemodynamics against clinical measurements was already performed [19] and model assumptions were shown to have only a minor impact on calculated hemodynamics [17,18]. Furthermore, a larger sample would be of great interest, because it would allow to evaluate effects of biological and mechanical prostheses separately. Since biological prostheses are nearly rotationally symmetric, it might be assumed that they are more robust to changes in the velocity inlet profile within the LVOT.

Finally, this study focused on the uncertainties introduced by only one aspect of the process pipeline of image-based, cardiovascular modelling: the patient-specific velocity inlet profile. There are, of course, several other possible sources of errors, as for example the reconstruction of the patient-specific anatomy from MRI image data or the uncertainties introduced by model assumptions, as for example neglecting the elasticity of the aortic wall or used turbulence models. Furthermore, the patient-specific MRI inflow profile itself is affected by errors due to image acquisition. The impact of these uncertainties is intensively investigated in several studies [4,12,13,33]. However, not only the main effects but also the interaction effects of those uncertainties on the prediction of hemodynamic outcome are of interest. A study, in which multiple uncertainties introduced during the process pipeline are compared, is desirable. Such a study would allow to identify, which aspects are most relevant for a reliable outcome prediction of cardiovascular intervention as the heart valve replacement.

5. Conclusions

In-silico methods and 4D-flow-MRI allow assessment of spatially resolved as well as averaged parameters, which might be correlated to a positive outcome of a valve replacement procedure within the future. However, these methods are relatively novel and have yet to be translated to clinical routine. Parameters correlated to the helicity of the ascending aortic blood flow, such as the SFD, are discussed to be associated with dilation of the ascending aorta. These parameters were robust against changes in the velocity inlet profile. Therefore, it might be possible to use simplified velocity inlet profiles, such as a plug profile, as boundary condition within patient-specific treatment-planning procedure using CFD.

This would be desirable, because it allows to circumvent two major problems regarding patient-specific simulations. The first one is that using a patient-specific velocity inlet profile requires 4D-flow-MRI data, which is not always available. A plug profile could be used while the volume flow rate could be estimated using general patient criteria such as age, weight, height and gender. The second problem, which could be circumvented, is that the replacement of the aortic valve will most likely result in a change of the ventricular function and thus a possible change of the velocity profile generated within the LVOT. There is no way to predict this change as of yet. Models that incorporate the ventricular motion might allow this prediction in the future. However, their application remains challenging due to their high computational cost. Since multiple interventions or surgeries have to be simulated to determine the

optimal patient-specific treatment, simplified approaches like the one presented in this study might be advantageous.

Acknowledgement

This work was funded by the German Research Foundation (IDs GO1967/6-1 and KU1329/10-1) and the European Commission (ID 611232). We would like to thank Alireza Khasheei for his work as MRI technologist.

References

[1] A.K. Attili, V. Parish, I. Valverde, G. Greil, E. Baker, P. Beerbaum, Cardiovascular MRI in childhood, Arch. Dis. Child. 96 (2011) 1147–1155, http://dx.doi.org/10.1136/adc.2009.179051.
[2] D.S. Bach, Echo/Doppler evaluation of hemodynamics after aortic valve replacement, JACC: Cardiovasc. Imaging 3 (3) (2010) 296–304, http://dx.doi.org/10.1016/j.jcmg.2009.11.009.
[3] H. Baumgartner, P. Bonhoeffer, N.M.S. De Groot, F. de Haan, J.E. Deanfield, N. Galie, M.A. Gatzoulis, C. Gohlke-Baerwolf, H. Kaemmerer, P. Kilner, F. Meijboom, B.J.M. Mulder, E. Oechslin, J.M. Oliver, A. Serraf, A. Szatmari, E. Thaulow, P.R. Vouhe, E. Walma, The task force on the management of grown-up congenital heart disease of the european society of cardiology, Eur. Heart J. 31 (2010) 2915–2957.
[4] S. Bozzi, U. Morbiducci, D. Gallo, R. Ponzini, G. Rizzo, C. Bignardi, G. Passoni, Uncertainty propagation of phase contrast-MRI derived inlet boundary conditions in computational hemodynamics models of thoracic aorta, Comput. Methods Biomech. Biomed. Eng. 20 (10) (2017) 1104–1112.
[5] N.S. Burris, M. Sigovan, H.A. Knauer, E.E. Tseng, D. Saloner, M.D. Hope, Systolic flow displacement correlates with future ascending aortic growth in patients with bicuspid aortic valves undergoing magnetic resonance surveillance, Invest. Radiol. 49 (10) (2014) 635–639, http://dx.doi.org/10.1097/RLI.0000000000000064.
[6] S. Chandra, S.S. Raut, A. Jana, R.W. Biederman, M. Doyle, S.C. Muluk, Fluid-structure interaction modeling of abdominal aortic aneurysms: the impact of patient-specific inflow conditions and Fluid/Solid coupling, J. Biomech. Eng. 135 (8) (2013).
[7] P.F. Davies, Hemodynamic shear stress and the endothelium in cardiovascular pathophysiology, Nat. Clin. Pract. Cardiovasc. Med. 6 (1) (2009), http://dx.doi.org/10.1038/ncpcardio1397.
[8] M.M. Dua, R.L. Dalman, Hemodynamic influences on abdominal aortic disease: application of biomechanics to aneurysm pathophysiology, Vascul. Pharmacol. 51 (2010) 11–21.
[9] K. Dumont, J. Vierendeels, R. Kaminsky, G. van Nooten, P. Verdonck, D. Bluestein, Comparison of the hemodynamic and thrombogeic perfomance of two bileaflet mechanical heart valves using a CFD/FSI model, J. Biomech. Eng. 129 (4) (2007) 558–565.
[10] M.D. Dyverfeldt, E.E. Hope, D. Saloner, Magnetic resonance measurement of turbulent kinetic energy for the estimation of irreversible pressure loss in aortic stenosis, JACC: Cardiovasc. Imaging 6 (1) (2013) 64–71, http://dx.doi.org/10.1016/j.jcmg.2012.07.017.
[11] P. Dyverfeldt, M. Bissell, A.J. Barker, A.F. Bolger, C.-J. Carlhäll, T. Ebbers, C.J. Francios, A. Frydrychowicz, J. Geiger, D. Giese, M.D. Hope, P.J. Kilner, S. Kozerke, S. Myerson, S. Neubauer, O. Wieben, M. Markl, 4D flow cardiovascular magnetic resonance consensus statement, J. Cardiovasc. Magn. Reson. 17 (2015) 72, http://dx.doi.org/10.1186/s12968-015-0174-5.
[12] V.G. Eck, J. Sturdy, L.R. Hellevik, Effects of arterial wall models and measurement uncertainties on cardiovascular model predictions, J. Biomech. 50 (2017) 188–194.
[13] O. Friman, A. Hennemuth, A. Harloff, J. Bock, M. Markl, H.O. Peitgen, Probabilistic 4D blood flow tracking and uncertainty estimation, Med. Image Anal. 15 (5) (2011) 720–728.
[14] A. Frydrychowicz, A. Berger, A. Munoz del Rio, M.F. Russe, J. Bock, A. Harloff, M. Markl, Interdependencies of aortic arch secondary flow patterns, geometry, and age analysed by 4-Dimensional phase contrast magnetic resonance imaging at 3 tesla, Eur. Radiol. 22 (2012) 1120–1130, http://dx.doi.org/10.1007/s00330-011-2353-6.
[15] D. Gallo, G. De Santis, F. Negri, D. Tresoldi, R. Ponzini, D. Massai, M.A. Deriu, P. Segers, B. Verhegghe, G. Rizzo, U. Morbiducci, On the use of In vivo measured flow rates as boundary conditions for image-Based hemodynamic models of the human aorta: implications for indicators of abnormal flow, Ann. Biomed. Eng. 40 (3) (2012) 729–741, http://dx.doi.org/10.1007/s10439-011-0431-1.
[16] J. Garcia, A.J. Barker, P. van Ooij, S. Schnell, J. Puthumana, R.O. Bonow, J.D. Collins, J.C. Carr, M. Markl, Assessment of altered three-dimensional blood characteristics in aortic disease by velocity distribution analysis, Magn. Reson. Med. 74 (2015) 817–825.
[17] L. Goubergrits, R. Mevert, P. Yevtushenko, J. Schaller, U. Kertzscher, S. Meier, S. Schubert, E. Riesenkampff, T. Kuehne, The impact of MRI-based inflow for the hemodynamic evaluation of aortic coarctation, Ann. Biomed. Eng. 41 (12) (2013) 2575–2587, http://dx.doi.org/10.1007/s10439-013-0879-2.
[18] L. Goubergrits, E. Riesenkampff, P. Yevtushenko, J. Schaller, U. Kertzscher, F. Berger, T. Kuehne, Is MRI-based CFD able to improve clinical treatment of coarctations of aorta, Ann. Biomed. Eng. 43 (1) (2015) 168–176.
[19] L. Goubergrits, E. Riesenkampff, P. Yevtushenko, J. Schaller, U. Kertzscher, A. Hennemuth, F. Berger, S. Schubert, T. Kuehne, MRI-Based computational fluid dynamics for diagnosis and treatment prediction: clinical validation study in patients with coarctation of aorta, J. Magn. Reson. Imaging 41 (2015) 909–916.
[20] F. Hellemeier, S. Nordmeyer, P. Yevtushenko, J. Bruening, F. Berger, T. Kuehne, L. Goubergrits, M. Kelm, Hemodynamic evaluation of a biological and mechanical aortic valve prosthesis using patient-specific MRI-Based CFD, J. Artif. Organs (2017), http://dx.doi.org/10.1111/aor.12955, ahead of print.
[21] K. Isaaz, J.F. Bruntz, A. Da Costa, D. Winninger, A. Cerisier, C. de Chillou, N. Sadoul, M. Lamaud, G. Ethevenot, E. Aliot, Noninvasive quantitation of blood flow turbulence in patients with aortic valve disease using online digital computer analysis of doppler velocity data, J. Am. Soc. Echocardiogr. 16 (9) (2003) 965–974.
[22] L. Itu, P. Sharma, K. Ralovich, Non-invasive hemodynamic assessment of aortic coarctation: validation with in vivo measurements, Ann. Biomed. Eng. 41 (2013) 669–681.
[23] S. Karimi, M. Dabagh, P. Vasava, M. Dadvar, B. Dabir, P. Jalali, Effect of rheological models on the hemodynamics within human aorta: CFD study on CT image-based geometry, J. Non-Newtonian Fluid Mech. 207 (2004) 42–52.
[24] M.R. Labrosse, C.J. Beller, F. Robicsek, M.J. Thubrikar, Geometric modeling of functional trileaflet aortic valves: development and clinical applications, J. Biomech. 39 (2006) 2665–2672.
[25] J.F. LaDisa, Jr., C.A. Figueroa, I.E. Vignon-Clementel, H.J. Kim, N. Xiao, L.M. Ellwein, F.P. Chan, J.A. Feinstein, C.A. Taylor, Computational simulations for aortic coarctation: representative results from a sampling of patients, J. Biomed. Eng. 133 (2001).
[26] X. Liu, Y. Fan, X. Deng, F. Zhan, Effect of non-Newtonian and pulsatile blood flow on mass transport in the human aorta, J. Biomech. Eng. 44 (2011) 1123–1131.
[27] R. Mahadevia, A.J. Barker, S. Schnell, P. Entezari, P. Kansal, P.W.M. Fedak, S.C. Malaisrie, P. McCarthy, J. Collins, J. Carr, M. Markl, Bicuspid aortic cusp fusion morphology alters aortic three-dimensional outflow patterns, wall shear stress, and expression of aortopathy, Circulation 129 (2014) 673–682, http://dx.doi.org/10.1161/CIRCULATIONAHA.113.003026.
[28] U. Morbiducci, R. Ponzini, D. Gallo, C. Bignardi, G. Rizzo, Inflow boundary conditions for image-based computational hemodynamics: impact of idealized versus measured velocity profiles in the human aorta, J. Biomech. 46 (2013) 102–109.
[29] C.D. Murray, The physiological principle of minimum work. I. the vascular system and the cost of blood volume, Proc. Nat. Acad. Sci. 12 (3) (1926) 207–214.
[30] S. Nordmeyer, E. Riesenkampff, D. Messroghli, S. Kropf, J. Nordmeyer, F. Berger, T. Kuehne, Four-Dimensional velocity-encoded magnetic resonance imaging improves blood flow quantification in patients with complex accelerated flow, J. Magn. Reson. Imaging 37 (2013) 209–216.
[31] C. Schmid, Leitfaden Erwachsenen Herzchirurgie, third ed., Springer, Berlin, 2014.
[32] M. Sigovan, M.D. Hope, P. Dyverfeldt, D. Saloner, Comparison of four-Dimensional flow parameters for quantification of flow eccentricity in the ascending aorta, J. Magn. Reson. Imaging 34 (2011) 1226–1230.
[33] J.S. Tran, D.E. Schiavazzi, A.B. Ramachandra, A.M. Kahn, A.K. Marsden, Automated tuning for parameter identification and uncertainty quantification in multi-scale coronary simulations, Comp. Fluids 142 (2017) 128–138.
[34] J. Ryval, A.G. Straatman, D.A. Steinman, Two equation turbulence modeling of pulsatile flow in a stenosed tube, J. Biomech. Eng. 126 (5) (2004) 625.
[35] T. Timmel, S. Seshadri, L. Goubergrits, K. Affeld, U. Kertzscher, Tri-Leaflet valve design with a purge flow for heart-Assist devices: an In-Vitro optimization study, Artif. Organs 36 (1) (2011) 42–48, http://dx.doi.org/10.1111/j.1525-1594.2011.01308.x.
[36] A. Updegrove, N.M. Wilson, J. Merkow, H. Lan, A.L. Marsden, S.C. Shadden, SimVascular: an open source pipeline for cardiovascular simulation, Ann. Biomed. Eng. (2016), http://dx.doi.org/10.1007/s10439-016-1762-8 (article in press).
[37] E. Wellnhofer, J. Osman, U. Kertzscher, K. Affeld, E. Fleck, L. Goubergrits, Flow simulation studies in Coronary arteries –impact of side-branches, Atherosclerosis 213 (2010) 475–481.
[38] P. Youssefi, A. Gomez, T. He, L. Anderson, N. Bunce, R. Sharma, C.A. Figueroa, M. Jahangiri, Patient-Specific computational fluid dynamics – assessment of aortic hemodynamics in a spectrum of aortic valve pathologies, J. Thorac. Cardiovasc. Surg. 153 (1) (2017) 8–20.
[39] W.A. Zoghbi, J.B. Chambers, J.G. Dumesnil, E. Foster, J.S. Gottdiener, P.A. Grayburn, B.K. Khandheria, R.A. Levine, G.R. Marx, F.A. Miller, Jr., S. Nakatani, M.A. Quinones, H. Rakowski, L. Rodriguez, M. Swaminathan, A.D. Waggoner, N.J. Weissman, Recommendations for evaluation of prosthetic valves with echocardiography and doppler ultrasound, J. Am. Soc. Echocardiogr. 22 (9) (2009) 975–1014, http://dx.doi.org/10.1016/j.echo.2009.07.013.

Jan Bruening is a PhD student at the Biofluid Mechanics Laboratory of the Charité – Universitätsmedizin Berlin. In 2008, he began working at the laboratory in 2008 during his bachelor studies of engineering science. During his bachelor and master studies at the Technische Universität Berlin, Germany, he focussed his work on cerebral aneurysms and rupture risk estimation using CFD. Beginning his PhD studies, his focus shifted toward aortic hemodynamics and virtual treatment planning using CFD.

Florian Hellmeier is a PhD student at the Biofluid Mechanics Laboratory of the Charité – Universitätsmedizin Berlin, where he studies medicine simultaneously. He received a Master of Science degree from the Technische Universität Berlin, Germany, as well as a Master of Science degree from the University of Michigan, USA. His research focus is assessment of cardiovascular hemodynamics using CFD as well as virtual treatment planning using image-based approaches.

Pavlo Yevtushenko is a master student at the Technische Universität Berlin and a student researcher at the Biofluid Mechanics Laboratory of the Charité – Universitätsmedizin Berlin. Besides his interest in cardiovascular research using CFD, he is interested in aerospace engineering and computational modelling as well.

Marcus Kelm is a paediatric cardiologist working at the Department for Congenital Heart Disease and Paediatric Cardiology of the Deutsches Herzzentrum Berlin, Germany. He focusses on translational research of cardiovascular modelling and the non-invasive acquisition of patient-specific profiles using MRI.

Sarah Nordmeyer is a paediatric cardiologist working at the Department for Congenital Heart Disease and Paediatric Cardiology of the Deutsches Herzzentrum Berlin, Germany. Her research focus is development of 4D-flow-MRI-based models for cardiovascular diagnostics and the clinical translation of those models.

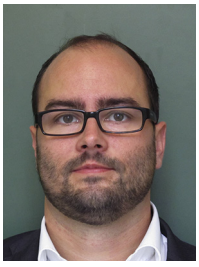

Simon Sündermann is an experienced heart surgeon and researcher at the Deutsches Herzzentrum Berlin, Germany. His research focuses are valve replacement and repair procedures as for example trans-catheter replacement of the aortic valve and repair of mitral valves.

Titus Kuehne is the director of the Institute for Computational and Imaging Science in Cardiovascular Medicine; Charité – Universitätsmedizin Berlin and head of the Cardiovascular Imaging group at the Congenital Heart Diseases department at the Deutsches Herzzentrum Berlin, Germany. The institute is focussing on research on patient-specific modelling at multiple biological scales as well as image-guided therapies.

Leonid Goubergrits is the head of the CFD working group of the Biofluid Mechanics Laboratory at the Charité – Universitätmedizin Berlin. During his more than 20-year-long experience in medical engineering he investigated several topics. His main interest, however, is to adapt numerical models in a way, that they might be used clinically. His current research focusses on cardiovascular hemodynamics as for example rupture risk estimation for cerebral aneurysms as well as developing virtual treatment models for patients suffering from congenital heart disease.